Measurement of correlated multiple light scattering in ultracold atomic ^{85}Rb

P. Kulatunga, C. I. Sukenik, S. Balik, and M. D. Havey
Department of Physics, Old Dominion University, Norfolk, Virginia 23529, USA

D. V. Kupriyanov and I. M. Sokolov
Department of Theoretical Physics, State Technical University, 195251 St. Petersburg, Russia
(Received 4 November 2002; published 29 September 2003)

We report an experimental study of correlated multiple light scattering in an ultracold gas of ^{85}Rb confined in a magneto-optic trap. Measurements are made of the polarization dependence of the spatial and spectral profile of light backscattered from the sample. The results show an interferometric enhancement sensitive to coherent multiple scattering in the atomic gas, and strong variations with the polarization of the incident and detected light. The spatial width and peak value of the enhancement are found to be dependent on the sample size. Comparison of all the measurements with realistic quantum Monte Carlo simulations yields a very good agreement.

DOI: 10.1103/PhysRevA.68.033816 PACS number(s): 42.50.Ct, 34.80.Qb, 42.25.Dd

I. INTRODUCTION

When electromagnetic radiation propagates in optically dense media, multiple scattering can dominate the transmission and scattering properties. For condensed systems, Mie scattering usually predominates, although Rayleigh scattering may be important for nanoscale materials. In general, the description of radiative transport in such media, which include a wide range of materials such as aerosols, turbid liquids, and disordered solids is often made with models assuming incoherent transport of the intensity of the electromagnetic wave. Wave transport, however, in which the phase of the wave is partially maintained even after multiple-scattering events, is important in many cases, and in fact, coherent radiative transport has been observed in solids, liquids [1,2], and in atomic gases [3]. In all these cases, there are correlations associated with multiple scattering of light, though the positions of the scatterers are uncorrelated, which survive configuration averaging. The earliest observations of coherent effects in radiative transport were of coherent backscattering [4–6], an effect in which light backscattered from a sample can originate from reciprocal, time-reversed paths inside the medium [1,2,7,8]. When the relative phases associated with the time-reversed paths are partially maintained, interference for light scattered into a narrow cone in the backward direction is observed. The appearance of the coherent backscattering (CBS) cone has been described as a weak localization effect for light [1,9]. Although no real localization is associated with this phenomenon, the appearance of the coherent backscattering effect is an indicator that coherent wave transport is occurring in the medium. It is believed that this process is of basic importance to the observation of true, or strong localization of light in a medium. There have been two recent reports of observation of strong localization of electromagnetic radiation [10,11]. In addition, lasing in random media, which may be considered as coherent radiative transport in a medium with gain, has been reported by several groups [12].

Atomic gases form a fundamentally and practically important medium in which the dynamics of coherent radiative transport and light localization can be studied. The existence of strong and spectrally narrow resonances allows the radiative transport properties of the medium to be readily studied over a wide range of optical depths. For example, excitation of the atoms near a resonance transition, and variation of the polarization of the exciting light, permits control of the scattering length and the tensor character of radiative transfer effects. Applied magnetic or electric fields may also be used to change both the mean-field character of the atomic vapor, as is often studied, or the light-scattering properties of the individual atoms. In addition, with increased light intensity, a perturbative description breaks down, and the physics of the atom-field system becomes much richer, even for scattering in optically thin atomic gases [13,14]. As discussed in more detail in the following section, there have been many studies of light propagation in optically dense atomic gases. However, the majority of these studies have been in thermal atomic gases, for which interpretation has focused on intensity transport through the sample. Over the last few years, considerable attention has been drawn to experimental measurements of coherent radiative transport in ultracold atomic gases. The first observations were made of the coherent backscattering effect in ultracold samples of ^{85}Rb confined in a magneto-optical trap [3]. Subsequently, fascinating studies have explored the geometrical and dynamic effects of applied magnetic fields on the spatial profile of the coherent backscattered light intensity [3,15,16]. In addition, recent theoretical efforts on wave transport in ultracold atomic gases by Müller *et al.* [17] and by our group [18] have focused on realistic modeling of some of the processes.

It is important to realize that light scattering in atomic vapors differs fundamentally from many studies in solid and liquid samples, even when the scattering centers in the latter case are sufficiently small that the scattering is primarily of the Rayleigh type. The first of these differences is that the radiative response of an atomic gas is characterized by relatively few strong and very-high-Q resonances. Second, the internal quantum states of the scatterers may be readily manipulated by the polarization of the radiation, thereby having a profound quantum statistical effect on observable interfer-

ences. Third, if the radiation initially incident on a sample has nonclassical features, then those properties themselves can be transferred to the atoms resulting, for example, in macroscopic entanglement of the sample [19]. In addition, and likely of essential importance to efforts to achieve strong localization of light in an atomic vapor, the properties of the scatterers themselves, and the subsequent scattered radiation, may be strongly modified by the radiation, leading necessarily to a nonlinear and many-body description of the process. In addition to playing the central role in the fundamental areas described above, including efforts to observe strong localization in an atomic medium, coherent multiple light scattering has important potential applications in several other areas of atomic and mesoscopic physics. These include intriguing magneto-optic effects [20] and the well-known dynamics and stability of ultracold confined atoms, such as atomic gases confined in a magneto-optic trap.

II. SCIENTIFIC PERSPECTIVE

In this section, we provide an overview of some radiative transport intensity effects in atomic gases which may be contrasted with the coherent wave transport effects which are the main focus of our studies. This will make clear some of the connections between the two, and also introduce some of the different phenomena which might be expected when coherent wave transport dominates the collective radiative properties of an atomic medium.

One of the most common descriptions of transport of radiation in atomic media is in terms of radiation trapping [21]. In this complex and generally nonlocal phenomenon, light is multiply scattered by atoms or molecules in an optically dense gas, leading to a slowing of the effective rate at which light energy is conveyed from one part of a sample to another. Among the more directly measurable effects are the lengthening of the observed radiative decay rate of atomic and molecular levels and complex distortion of the spectral profile of radiation emerging from the vapor. Various theoretical descriptions are available through, for example, the Holstein equation or through radiative transport equations of the processes [21]. The problem is made particularly difficult because of spectral redistribution of light as it propagates through the vapor. For a thermal atomic gas, redistribution is dominated by collisions, by Doppler shifts associated with absorption and reemission of the light, and by inelastic radiative transitions in the atomic medium. An important fundamental limitation of many descriptions of radiative transport is the neglect of interferences associated with coherent transport of the electromagnetic wave through the medium, rather than the intensity of the associated wave. These effects are expected to appear in several circumstances: (a) when there is recurrent scattering in the vapor, (b) when higher-order correlations in light scattering are measured, and (c) when interferometric observables are directly studied, such as in the coherent backscattering effect. Phenomena associated with this are to some extent related to the partial frequency redistribution of radiation in scattering from an atomic resonance line [21]. However, for the scattering of weak field and nearly monochromatic classical radiation from an atomic line, the scattering in the atom's rest frame is always coherent, so long as collisions may be neglected. To describe this more clearly, it is necessary to specify what is meant by coherent transport, particularly in relation to other coherent effects that frequently are observed in atomic vapors.

First of all, we consider continuous and very nearly monochromatic but weak incident radiation having a spectral width much narrower than a characteristic atomic line width. Under these circumstances, the radiation undergoes quasielastic scattering in the atomic rest frame, with only a normally small recoil shift in the atomic energy. In the laboratory frame, however, there are frequently large Doppler shifts associated with both the incoming and outgoing radiation fields, and there are also phase shifts that generally depend on the atom velocity in the laboratory. For light that is multiply scattered in a thermal atomic vapor, these shifts lead generally to dephasing and redistribution of the radiation; the interferences associated with wave scattering then often do not survive configuration averaging. Second, there are well-known effects that are related to radiation trapping in a vapor, and which also depend on coherent evolution of atomic observables in applied magnetic fields. In several circumstances, including those associated with the Hanle effect and with double-resonance experiments, the phenomenon of ''coherence narrowing'' directly results from multiple scattering in the vapor [22]. A similar effect also occurs in the coherent evolution of the atomic orientation. Higher-order electronic multipoles may be created, and should have a dynamical narrowing associated with them, but these do not normally play a role in atomic dipole radiation, a situation frequently of importance in radiative transport.

With this background, coherent radiative transport can generally be understood as the transport of wave amplitude (rather than intensity) through an atomic vapor. The fundamental difference between wave amplitude radiative transport and wave intensity transport is that there are interferences which appear in the total intensity, and which can have profound influence on the radiative properties of the system. When stochastic phase and frequency shifts associated with the physical system become large, or are not in some way compensated for, the interferences do not survive configuration averaging, and a classical radiative transport equation results in a proper theoretical description of the dynamics of wave intensity in the system. However, there are circumstances when the interferences do survive averaging over unselected variables, and it is these situations that concern us here.

In the present work, the principal observable is the coherent backscattering effect, which is a definitive and striking characteristic of coherent radiative transport of light in a medium. In coherent backscattering, radiation follows reciprocal multiple-scattering paths through a medium. For a semi-infinite medium, it is straightforward to show that the geometric phase difference accumulated on a multiple-scattering path is given by [1,9]

$$\Delta\phi = (\mathbf{k}_i + \mathbf{k}_s)\cdot(\mathbf{r}_f - \mathbf{r}_l).$$

In the equation, $\mathbf{k}_i$ and $\mathbf{k}_s$ are the wave vectors of the

incident and scattered light, while $\mathbf{r}_f - \mathbf{r}_l$ is the spatial separation between the first and last scatterers. In the backscattering direction $\mathbf{k}_i + \mathbf{k}_s = 0$, and so the accumulated phase difference is zero. Averaging over all possible paths resulting in the same value of $\mathbf{r}_f - \mathbf{r}_l$ gives a characteristic and well-understood cone-shaped spatial profile associated with the backscattered light. This profile, including its amplitude relative to an incoherent background and its general shape, depends on the mean length of a multiple-scattering path in the medium and on the permitted Rayleigh, elastic Raman, and inelastic Raman transitions in the atom. It should also be pointed out that there are other experimentally accessible observables [23,24], including the noise spectrum associated with scattered light, which may serve as indicators of coherent radiative transfer; we focus here on the coherent backscattering effect.

In a CBS experiment, the intensity of light scattered by a sample is measured for a range of scattering angles in the nearly backward direction. In the direct backward direction, the angle θ between $\mathbf{k}_i$ and $\mathbf{k}_s$ is π, making the phase $\Delta\phi = 0$ and constructive interference maximum. Away from the backward direction, the interference terms go to 0 when the phase $\Delta\phi \sim \pi$, leaving a so-called incoherent background. It is important to realize that this background can have strong variations in intensity due to multiple coherent scattering from a single configuration of scatterers. This single- and multiple-scattering speckle disappears upon configuration averaging, leaving only the coherent backscattering cone. There are generally three contributions to the backscattered radiation, these being the single-scattering intensity I_s, and the so-called ladder (I_l), or direct terms and the crossed (I_c), or interference terms. From these quantities it is customary to define an enhancement E as the ratio of the total intensity to the sum of the ladder plus single-scattering intensities. For classical scatterers the maximum value of the enhancement is $E = 2$. However, for mesoscopic atomic samples, the enhancement (and spatial width) depends sensitively on the physical size of the sample.

In this paper, we describe in detail experiments on correlated multiple light scattering in an ultracold gas of atomic ^{85}Rb. In the present studies, the spatial and polarization dependences of the conical backscattering signal are measured for a well-characterized sample of ultracold ^{85}Rb atoms confined in a magneto-optic trap. Detailed description of the experimental arrangement and protocols is also given. Original measurements of these quantities, also in an ultracold gas of atomic ^{85}Rb, were reported by Labeyrie *et al.* [3]. However, in those experiments the atomic sample had a significantly larger spatial size and contained an order of magnitude more atoms, thus having several times the optical depth, in comparison with the data reported here. Even though the atomic constituents are the same, these are nontrivial differences for mesoscopic samples where the observables, such as the coherent backscattering, depend on the fact that the coherence extends over the full size of the atomic sample. In fact, as shown experimentally here (by comparison with the results of Labeyrie *et al.* [3]) both the spatial width of the atomic backscattering cone and the enhancement depend on the atomic spatial density distribution and on the optical depth. To extract the dependence on the mesoscale variables, we have made absorption measurements of the on-resonance optical depth and characterized the spatial atom distribution by fluorescence imaging. In addition, we have measured, in the helicity channels, the spectral variation of the total intensity of coherent plus incoherent light scattered from the sample. These variations also depend on sample size and optical depth, but have only a small contribution due to the coherent backscattering cone.

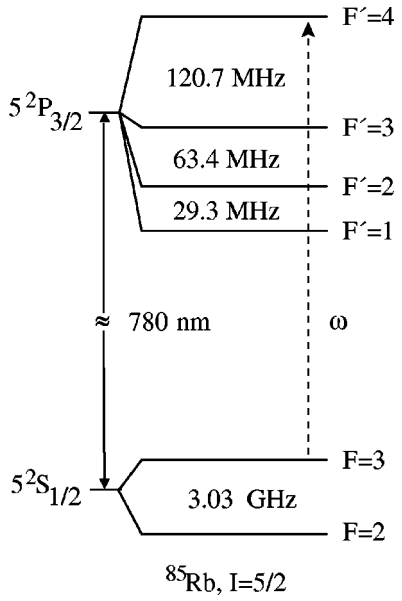

FIG. 1. Partial energy-level diagram showing relevant transitions in the $D2$ hyperfine manifold of ^{85}Rb.

Finally, the spatial and polarization variations of the backscattered light, including the CBS cone region, are then compared with quantum Monte Carlo simulations of the process [18], these being done for physical conditions closely matched to those of the experiments. We point out that the theoretical development of the simulations has been previously reported [18], and also the quality of the results established by comparison with the experimental coherent backscattering cone shape in the lin $\perp$ lin polarization channel. In this paper, we present further results comparing experiment and simulation for all four standard polarization channels (as defined in the following section), on the spatial variation of the total backscattered intensity in the vicinity of the $F = 3 \rightarrow F' = 4$ hyperfine transition. The nontrivial polarization variations are due to the interplay between atomic Rayleigh and Raman transitions in multiple scattering, and also depend significantly on atomic sample size and optical depth.

III. EXPERIMENTAL APPROACH

An energy-level diagram of the hyperfine transitions relevant to the experimental scheme is shown in Fig. 1. A schematic diagram of the instrumentation used in the experiments is shown in Fig. 2. The CBS external light source used in the experiment is provided by an external cavity diode laser (ECDL) that is stabilized by saturated absorption to the excited-state hyperfine $F = 3 \rightarrow F' = 2,4$ crossover resonance

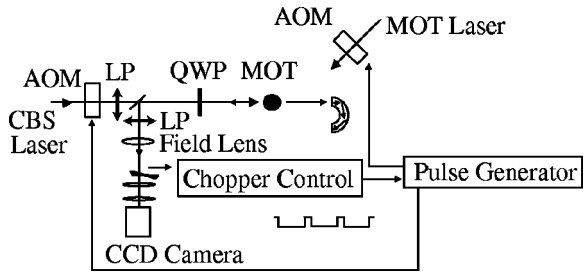

FIG. 2. Schematic diagram of the experimental apparatus, showing the relative layout of the coherent backscattering polarimeter and the ^{85}Rb magneto-optic trap containing the ultracold atomic scattering sample. Devices in the figure include an acousto-optic modulator (AOM), linear polarization analyzer (LP), a quarter-wave plate (QWP), a charge-coupled device camera (CCD), and the coherent backscattering laser (CBS). The magneto-optic trap is labeled as MOT.

associated with the $5s^2\,S_{1/2}\rightarrow 5p^2\,P_{3/2}\;D2$ transition. Here $F(F')$ refers to the ground (excited) level hyperfine manifold. In general, the CBS laser may be tuned several hundred MHz from nearly any hyperfine resonance in either ^{85}Rb or ^{87}Rb by a standard offset locking technique using an acousto-optic modulator. In the experiments described in this paper, the CBS laser is varied within a few linewidths of the $F=3\rightarrow F'=4$ hyperfine transition. The laser bandwidth is a few hundred kHz, much narrower than the natural width $\sim$5.9 MHz, and the typical output power is about 5 mW (this is attenuated significantly in order to have a on-resonance saturation parameter of about 0.01). In order to produce a nearly Gaussian beam profile, the laser output is launched into a single-mode polarization-preserving fiber and then the beam is expanded and collimated to a $1/e^2$ diameter of about 8 mm. The collimation of the CBS beam is confirmed with a shear-plate interferometer. The polarization of the resulting beam is selected and then the beam passed through a nonpolarizing, wedged and nominally 50-50 beam splitter that passes approximately half of the laser power to the atomic sample. The radiation backscattered from the atomic sample is directed by the same beam splitter to an antireflection-coated achromatic doublet field lens of 45 cm focal length, which focuses the light onto the blades of a mechanical chopper. A pair of achromatic doublet transfer lenses then recollects the light and brings it to the focal plane of a liquid-nitrogen-cooled charge-coupled device (CCD) camera. The diffraction limited spatial resolution is about 100 μrad, while the polarization analyzing power at 780 nm is on the order of 5000 for the circular polarization channels and 15 000 for the linear ones. The unused beam reflected from the beam splitter, and the portion of the CBS beam that passes through the magneto-optic trap (MOT) chamber are directed to beam dumps. The dumps are specially designed to minimize backscattering of light to the detector. They consist of a dielectric glass filter, which is strongly absorbing at the CBS laser wavelength of 780 nm, inserted at Brewster's angle. The residual reflected radiation is directed to a flat-black foam absorber, while the transmitted radiation is dissipated in a flat-black painted Cu tube. With these precautions, laser radiation scattered from the beam dumps is reduced to negligible levels.

The sample of ultracold ^{85}Rb atoms is formed in a vapor-loaded MOT, which is operated in a standard six-beam configuration on the closed $F=3\rightarrow F'=4$ hyperfine transition. The main MOT laser beams are derived from a stabilized ECDL master-slave arrangement and formed into three pairs of retroreflected beams, each having a power of approximately 3.3 mW. Hyperfine repumping to accommodate the weak leak to the $F=2$ ground level is achieved by microwave modulation of the slave laser to generate a sideband at the $F=2\rightarrow F'=3$ transition frequency. The MOT lasers may be redirected away from the fiber launcher by an acousto-optic modulator placed after the slave laser. The combination has an effective attenuation of about 65 dB.

Fluorescence imaging of the MOT showed that it was approximately ''cigar shaped,'' having $1/e$ Gaussian radii of about 0.55 mm and 0.69 mm. The radius r_0 is defined in terms of a Gaussian atom distribution $n(r)$ according to $n(r)=n_0\exp(-r^2/2r_0^2)$, where n_0 is the peak density in the MOT. For this distribution, the optical depth b is related to r_0 according to $b=\sqrt{2\pi}\,\sigma_0\,n_0\,r_0$, where σ_0 is the cross section for light scattering [18]. For the present experiment, we determine the optical depth by direct measurement of the transmitted CBS light intensity, which is attenuated as e^{-b}. For the present trap, the resulting ^{85}Rb sample has a peak density of about 3×10^{10} atoms cm^{-3} and an optical depth through the trap center of about 6. The sample temperature is measured by a time-of-flight technique to be less than 50 μK.

For the experiments described here, where the signal consists of light backscattered from the atomic sample, it is critical to minimize the influence of the windows used for directing the CBS laser beam through the chamber and for detecting the subsequent scattered light. To minimize direct reflections from the MOT windows, they are V coated at 780 nm, having thus a reflectivity per surface of about 0.25%. To suppress further reflections from the entrance window, where the CBS beam enters the MOT chamber, the window is mounted on a vacuum bellows, allowing us to direct the residual reflections outside the light collection apertures. Finally, to eliminate fringe formation in the focal plane of the CCD camera, it is necessary to also use a 1° wedged light collection window on the MOT vacuum chamber.

There are four polarization channels that are customarily studied in coherent backscattering. For linearly polarized input radiation, two of these correspond to measuring the backscattered light in two mutually orthogonal output channels. These channels are customarily labeled as lin $||$ lin and lin $\perp$ lin. Measurement in these channels is readily achieved by removing the quarter-wave plate, shown in Fig. 2, and rotating the linear polarization analyzer located before the field lens. For input radiation of definite helicity, which being generated by the linearly polarized input and the quarter-wave plate, the helicity of the backscattered radiation is similarly measured by rotation of the linear polarizer before the field lens. The two channels in this case correspond to measurements in the helicity preserved channel $(h||h)$ and helicity changed channel $(h\perp h)$. Note that these polarization states do not completely describe the backscattered radiation, un-

less observations are made in the exact backscattering direction. In general, there are four Stokes (or equivalent) parameters required to describe the light, and in this case there are only three for each input polarization state. For example, for light of definite helicity incident on the atomic sample, a linearly polarized backscattered component is possible when observations are made off the exact backscattering direction. However, to make comparison with other results, we have confined here our measurements to the four customary channels.

The performance of the coherent backscattering polarimeter is first assessed by measuring how well the CBS laser beam is brought to a focus on the CCD camera detector array when a flat mirror is used in front of the sample chamber. This measurement showed that the minimum spot size corresponded to a spatial resolution of about 100 μrad, which closely matches the diffraction limit for the optical system. The instrument was also used to measure the width of the coherent backscattering cone from dilute liquid suspensions of TiO_2 in water. As the width of the CBS cone is inversely proportional to the mean free path of light in a sample, sequentially tittering the suspension showed again that the spatial resolution is on the order of 100 μrad.

As a third and most direct test of the combined instruments used in the experiments, we measured directly the interaction of the coherent backscattering laser with ultracold ^{85}Rb atoms confined in the MOT. The interaction of the coherent backscattering laser, tuned in the vicinity of the $F=3\rightarrow F'=4$ hyperfine transition, generates an intense near-degenerate four-wave mixing signal when the MOT lasers are on. The angular spread of the degenerate four-wave mixing signal from the trapped Rb atoms, which is generated by pairs of the MOT laser beams and the CBS beam interacting with the cold atoms, is $\sim$100 μrad, consistent with the direct reflection measurements described earlier. Although consistent with measurements made using the other two methods, the phase-matching condition for the four wave mixing implies that the exact angular position and width also depend on the MOT laser beam alignment and so is somewhat sensitive to the exact alignment of the MOT. It is also interesting to note that for ideal standing waves set up by the MOT lasers, the phase-matching condition for degenerate four-wave mixing is the same as that for the CBS cone. This circumstance permits convenient and quite precise positioning of the peak cone intensity on the CCD detector array.

The main measurement goal of the experiment is to determine the angular, spectral, and polarization dependence of the probe CBS light backscattered from an ultracold sample of ^{85}Rb atoms. To accomplish this, the general data-taking protocol is to alternately switch on and off the MOT and CBS lasers, thus measuring the scattered light from atoms undisturbed by the MOT lasers. Switching is accomplished by using acousto-optic modulators to suppress the coupling of the laser light into the fiber optic cables directing the MOT and CBS laser beams to the sample. The timing is synchronized by a chopper in the CBS detection arm; the complete timing cycle is shown in Fig. 3. The chopper is required to gate the CCD detector, protecting it from the intense trapping laser light scattered by the Rb sample when

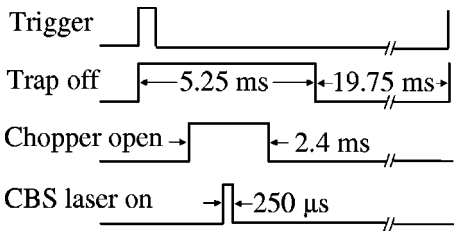

FIG. 3. Diagram showing the relative timing protocol for the coherent backscattering experiments.

the MOT lasers are on. This is the technique employed by Labeyrie *et al.* [3] in the original atomic CBS experiments. By adjusting the relative phase of the chopper and the MOT laser acousto-optic modulation, signals from the trapping phase may be completely eliminated from the CBS data phase. The full data-taking duty cycle is 1%, this being when the chopper is open to receive CBS scattering signals from the ultracold Rb sample, and the CBS laser is directed toward the sample. The remaining part of the cycle is used for adjusting the chopper-open phase and for reconstituting the MOT, preparing it for the next data cycle. In a typical 300-s run, the signal due to light backscattered from the sample is on the order of 500 counts per pixel. In addition to this desired signal, there are background signals from light scattered off components of the apparatus and from fluorescence due to hot ^{85}Rb atoms excited by the CBS laser. The total background due to these sources is about 300 counts, with the major part $\sim$150 due to scattering of CBS laser light from hot rubidium atoms in the chamber. The background signal is measured by repeating the timing protocol above, but with the current to the MOT field gradient coils turned off. A single run consists of 300-s total signal and background runs, with the final measurement consisting of the difference between the two. Typically ten or more runs are accumulated in order to provide good statistics for further analysis of the backscattering line shape and intensity.

Finally, there are several other elements of the experiment that are critical for avoiding systematic errors in the measurements. First of all, the CBS laser beam should be nearly centered on the sample of cold atoms, as variations in the wave-front amplitude across the cold atom sample can adversely affect the backscattering enhancement [3]. In practice, this is accomplished by looking at the shadow of the MOT in the transmitted CBS beam and centering the shadow in the central part of the beam. Second, it is important that the CBS laser does not disturb significantly the Rb sample during the data-taking phase. This is because the coherent backscattering line shape for small samples depends sensitively on the optical depth [3], on the size of the sample [18], and on the motion of the atoms in the sample [3]. The main effects occur because the CBS laser accelerates the atoms along its direction, with a maximum saturation acceleration $\sim 10^5$ m/s^2. This puts constraints on the length of time that the atoms are exposed to the CBS laser beam and also on the intensity of the beam. During the data-taking cycle, the CBS laser beam is switched on for 0.25 ms and the on-resonance saturation parameter is limited to a maximum of 0.01, limit-

ing the maximum velocity and displacement of the atoms to acceptable levels.

IV. SIMULATION OVERVIEW

We have previously reported the details of a Monte Carlo simulation [18] of coherent multiple light scattering in ultracold atomic Rb. In that paper, the fundamental governing equations were developed, and the simulation of the light scattering was used to predict the width and enhancement of the coherent backscattering cone under a variety of conditions. The quality of the simulations was tested by comparison with our earlier experimental results in the lin $\perp$ lin polarization channel. Here we quite briefly describe how the simulations were done, referring the reader to our published work for details. As was discussed above for light scattered by the sample in the backward direction, there are two contributions in the energy flux, which are, respectively, called ladder-type and crossed- or interference-type contributions. For atomic light scattering in an ultracold gas, the interference terms survive configuration averaging, and are responsible for the CBS phenomenon. In our simulation procedure, we randomly choose any chain of scatterers of a certain scattering order, and then calculate both the ladder and interference contributions to the scattered light intensity. To describe the propagation of the light wave in the sample between the scatterers as well as its propagation on incoming and outgoing paths, we used the formalism of the Green propagation function. For elastic scattering on cold atoms and after mesoscopic averaging, this approach leads to the well-known Bouguer-Lambert law for attenuation of the wave, and also to proper description of the phase accumulation in the effective atomic medium. Repeating the simulation procedure many times, we averaged the contributions over such randomly chosen chains of the atomic scatterers and finally obtained a reliable estimation of the output light intensity which actually accumulates all the possible scattering chains. Starting from single and double scattering, we extended our procedure up to the higher orders where the partial contributions to the output intensity became negligible. Normally for a spatially symmetric or close to symmetric atomic cloud, the procedure can be truncated when the scattering order is approximately twice as large as the optical thickness of the sample. In the present case, that is about 12 orders of scattering. The theoretical approach also analytically accounts for the Zeeman degeneracy of the ground and excited levels, and for inelastic Raman transitions due to the off-resonance $F=3\rightarrow F'=2,3$ hyperfine transitions.

V. RESULTS

Images of the spatial distribution of backscattered light in the four standard polarization channels and for resonant excitation on the $F=3\rightarrow F'=4$ hyperfine transition are shown in Fig. 4. With reference to the figure, and as discussed earlier, these channels are customarily labeled as (a) lin $||$ lin, (b) lin $\perp$ lin, (c) $h||h$, and (d) $h\perp h$. The images are color coded to indicate by white and red the regions of peak intensity, and blue and black the regions of lesser intensity, these areas being evident in the figure. The region of peak intensity is customarily called the ''cone,'' even though line scans through the angular distribution are more nearly Lorentzian than conical, and do not show the cusp-shaped peak characteristic of coherent backscattering from a semi-infinite medium. This is not due to the finite spatial resolution of the instrumentation, but instead because very long multiple scattering paths are necessary to generate the sharp conical spatial feature.

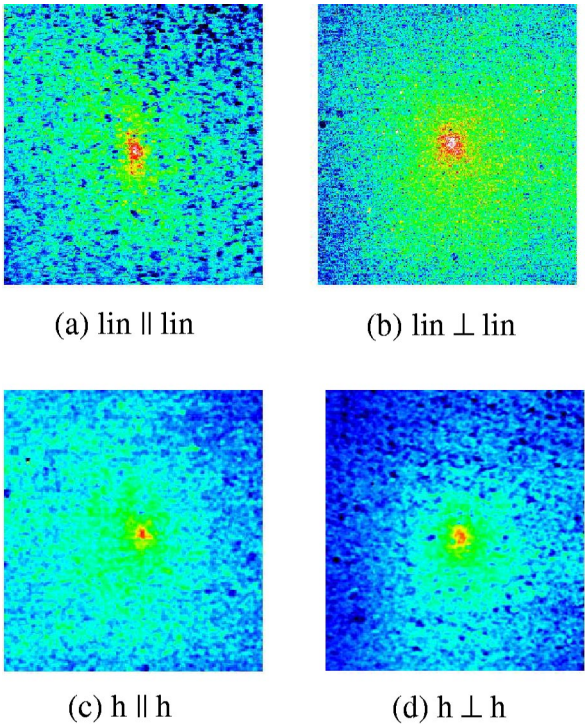

FIG. 4. Intensity diagrams showing the spatial variation of backscattered light, including the cone region, for four polarization channels. The data correspond to an approximately 15×15 mrad^2 detection solid angle. (a) lin $||$ lin, (b) lin $\perp$ lin, (c) $h||h$, (d) $h\perp h$.

Each of the CBS images in Fig. 4 corresponds to an average intensity of several thousand counts per pixel. These characteristically represent an accumulation of 10–20 individual data runs. However, the color-coded intensity scale in Fig. 4 has been amplified to bring out features associated with the cone region. This also brings out residual speckle noise present in three of the four polarization channels. This appears because there is background due to stray light scattered off instrumental elements, including the quarter-wave plate used in the helicity channels. Slight variations in the configuration of the experimental apparatus during the course of data taking and background subtraction lead to residual speckle that is not completely eliminated by background subtraction. This is nearly absent in the lin $\perp$ lin channel because the quarter-wave plate is not used, and because detection polarization analysis suppresses most of the remainder. In spite of this, the spatial asymmetries present in the linear polarization channels are evident in the images. These include the greater cone width in the vertical direction for the lin $||$ lin channel and the lines of symmetry along the bisectors of the incident and detected linear polarization di-

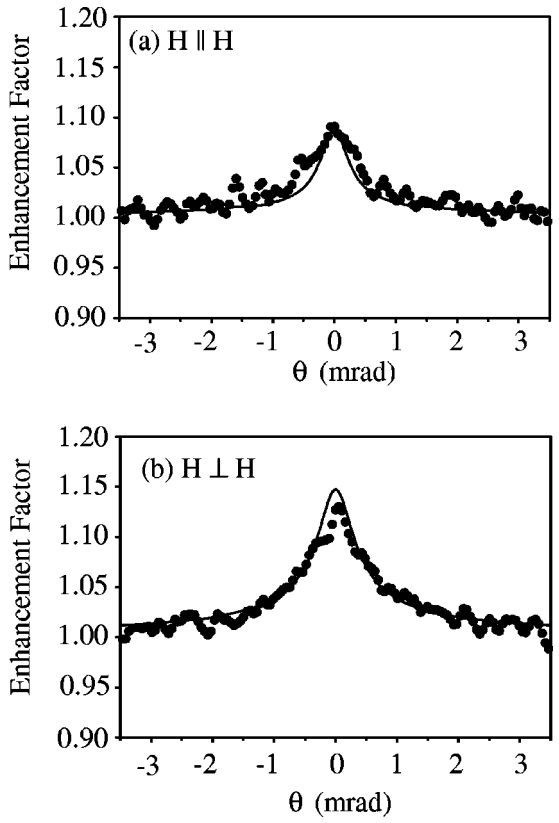

FIG. 5. Line scans through the CBS cone for the (a) $h||h$ and (b) $h\perp h$ polarization channels. The solid curves are the result of quantum Monte Carlo simulations of the CBS process for the corresponding polarization channel.

rections in the lin $\perp$ lin channel. Each of these is discussed further below.

To illustrate the cone profile, we present in Fig. 5 line scans of the spatial intensity distribution through the center of the cone for the helicity preserving and helicity nonpreserving polarization channels. For excitation and detection of light of definite helicity, the intensity is not expected to depend on the angular displacement around the direction of the incident wave vector. We point out that, in final quantitative data analysis, to extract the enhancement and cone widths, the intensity profile is reduced by angular integration, about the wave vector of the incident light, of the corresponding data in Fig. 4. This procedure improves significantly the signal-to-noise ratio for the wings of the cone, but does not greatly improve the determination of the peak intensity at the center of the cone. For the line scans shown in Fig. 5, we have not integrated the data; as seen from the line scans the cones have an angular width of about 1 mrad, and enhancements that are typically less than 15%.

Also shown in Fig. 5 is a direct comparison (not a fit) with quantum Monte Carlo simulations of the coherent backscattering spatial profile [18]. The simulations are done for conditions closely resembling those in the experiments. In particular, an asymmetric Gaussian atom distribution with Gaussian dispersions of 0.55 mm and 0.69 mm and with a maximum optical depth of 5 is selected for the simulation. The multiple scattering simulations are done for weak incident fields, where saturation and correlation are negligible. Scattering orders of more than ten are necessary in order to obtain convergence of the width and the enhancement. In comparisons of the experimental results and the simulations, there are two general elements to consider. The first of these is the enhancement, which is quite sensitive to the polarization channel, and increases weakly with density at fixed sample dimensions. The width of the cone, on the other hand, is strongly dependent on the size of the sample, with the width increasing nearly linearly with the inverse size of the sample [18]. Qualitatively, this is because the cone width is sensitive to the average location of the first and last scatterers associated with reciprocal paths, in the same way that the fringe frequency in a double slit is sensitive to the slit separation. To obtain the very good agreement seen in Fig. 5, and in comparisons to follow, it is then necessary to have careful measurements of the MOT size and approximate measures of its shape. The quantitative agreement between the experiment and the simulations shows that such measurements can lead to inference of the average sample size from the CBS measurements. We point out that varying the effective sample size by detuning the scattering radiation from exact resonance is not strictly equivalent to changing the physical sample size. The reason for this is that there are variations in the backscattering interferences from off-resonance hyperfine transitions; in the present case, these are due to the off-resonance $F=3\rightarrow F'=2,3$ transitions.

In Fig. 6, we present similar scans, but for the two linear polarization channels. These data are typically noisier than the other polarization channels because of speckle noise present in the environmental background light. As discussed earlier, slight variations in the speckle during the course of experimental runs lead to the variations shown. For the lin $||$ lin polarization channel, the cone spatial line shape does not generally possess axial symmetry about the direction of the incident wave vector. Thus we present in the figure both horizontal and vertical scans across the cone, where a horizontal scan corresponds to a direction perpendicular to both the incident wave vector and the direction of the incident electric-field vector. In spite of the speckle noise in the data, the spatial asymmetry is clear in the lin $||$ lin channel, where the cone width is approximately two times wider for a vertical scan than for a horizontal one. A physical reason for this is that the scattering of linearly polarized light on the $F=3\rightarrow F'=4$ transition is preferentially directed perpendicular to the direction of the incident polarization, as expected for electric dipole radiation from an aligned system. Multiple scattering magnifies this propensity, and this makes the multiple scattering strongly localized in a horizontal plane. Thus the first and last scatterers in a multiple-scattering sequence lie to a good approximation along lines perpendicular to the incident polarization direction, and the phase associated with the detected light will vary relatively rapidly in that direction. However, the phase will vary much more slowly in the vertical direction, in direct analogy to the interference fringes formed from a horizontal double pin hole, and the resulting cone will be significantly wider than that in the horizontal direction. As shown by the solid lines in Fig. 6, this behavior is again in very good agreement with theoretical simulations.

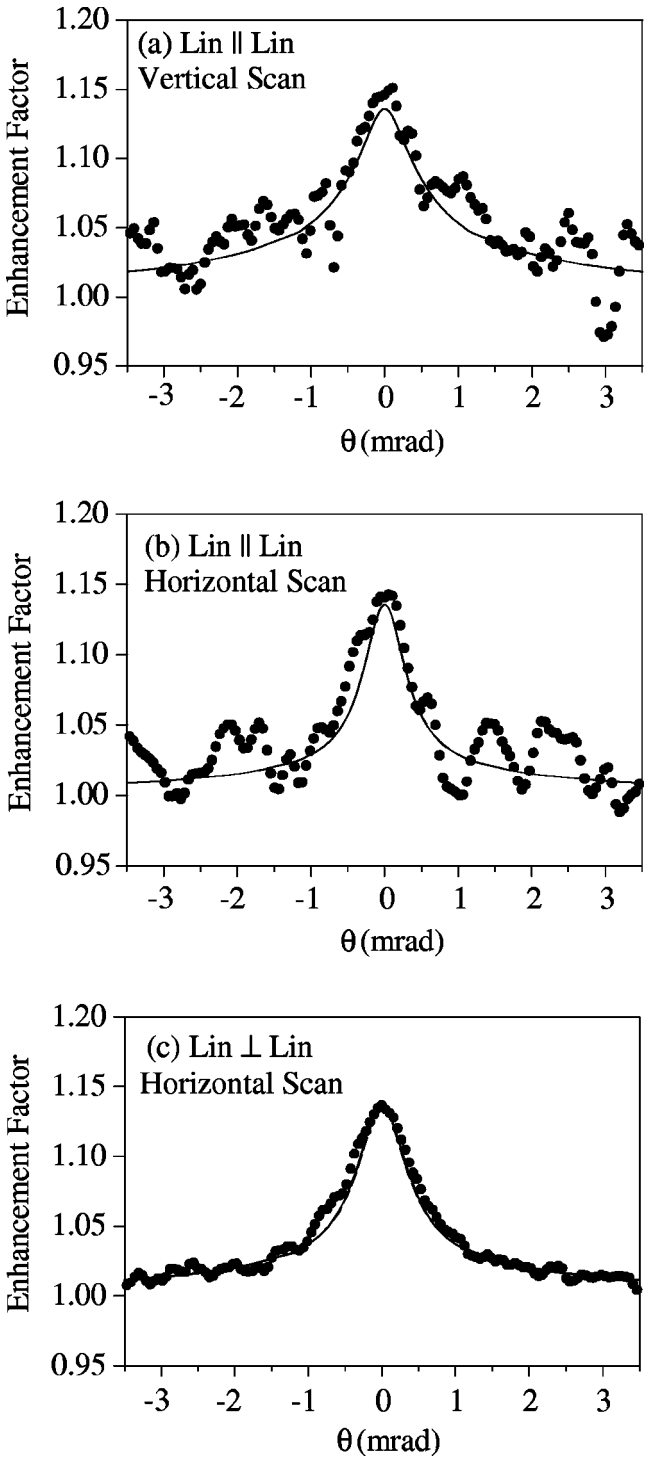

FIG. 6. Line scans through the CBS cone for the (a) lin || lin (horizontal scan), (b) lin || lin (vertical scan), and (c) lin ⊥ lin horizontal scan. In each case, results of quantum Monte Carlo simulations are indicated by solid lines.

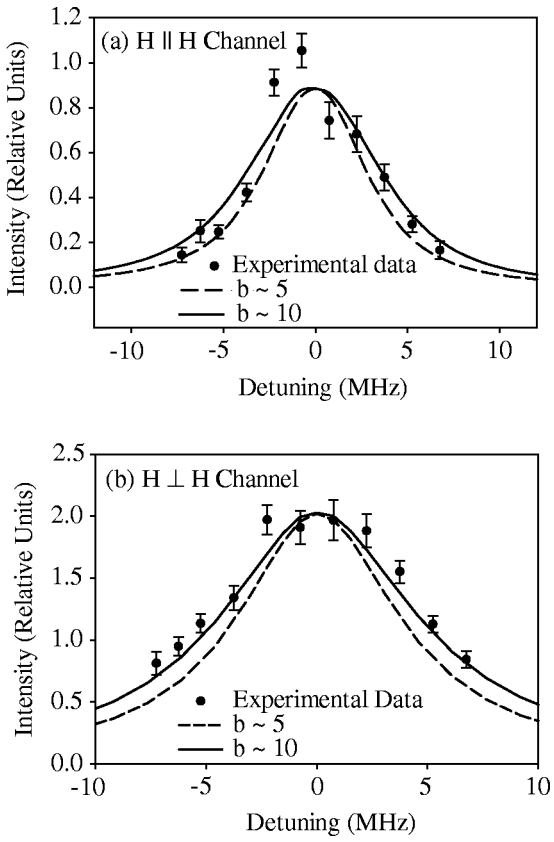

FIG. 7. Experimental and theoretical results for the total intensity of light backscattered from the ultracold Rb sample. Data for the two helicity polarization channels are shown.

For the lin ⊥ lin polarization channel, there is a related symmetry, but one that does not arise directly from the angular distribution in single scattering of light linearly polarized perpendicular to the incident light, as this distribution is necessarily isotropic. Instead it comes from the component of light perpendicular to the incident polarization generated by solely multiple scattering. As may be readily seen for linearly polarized light exciting an array of classical oscillators, this contribution to the scattering has a maximum contribution in directions bisecting the horizontal and vertical directions, as recently demonstrated in CBS experiments in ultracold strontium atoms [25].

From the data in Figs. 5 and 6, we see that the interferometric enhancement is on the order of 1.15 (15%), relative to the incoherent background, for all four polarization channels. This enhancement should be compared with what is expected, and seen for coherent backscattering from classical scatterers, including light scattered from ultracold Sr atoms on the $^1S_0 \rightarrow {}^1P_1$ resonance transition. In that case, for the helicity preserving $(h||h)$ channel, single scattering is absent, and so the enhancement should be 2. It was first discovered by Labeyrie *et al.* [3] that the enhancement in ultracold Rb is significantly less than this. Generally, the physical origin in the present case lies in the internal atomic hyperfine structure, which permits elastic and inelastic Raman transitions as well as Rayleigh scattering of monochromatic light from the atoms. As discussed by Müller *et al.* [17], it is atomic transitions to a distribution of magnetic sublevels along a multiple-scattering path that leads to an imbalance in the direct and reversed scattering amplitudes, and thus to a reduction in the overall enhancement. On the other hand, we reemphasize that the ~1-mrad width of the cone is significantly larger in the present work than that reported earlier

[3,17]. As pointed out in previous paragraphs, this is not due to a difference in spatial resolution in the measurements but instead arises from the sample-size dependence of this quantity.

Finally, we have also measured and simulated the spectral variation of the relative total intensity of light backscattered into a 20×20 μrad^2 cross section centered on the cone region around $\theta=0$ mrad. This quantity depends very weakly on interference effects in the radiative transport, for the majority of this signal corresponds to the incoherent background. Representative data, corresponding to the two helicity polarization channels, is shown in Fig. 7. There it is seen that the spectral width is several times the natural width associated with single scattering. This occurs because the sample is optically thick; even when the CBS laser is spectrally detuned an amount larger than the natural width, the light penetrates further into the sample but is still scattered and can contribute to the intensity emitted from the sample. It is only when the detuning is so large that the optical depth becomes significantly less than unity, that the scattering line shape will reduce to that for single scattering. This broadening may alternately be related to the increase of the width of the absorption profile in forward-scattered light, and may be similarly modeled to obtain the qualitative effect. Also shown in Fig. 7 is the result of simulations of the spectral behavior. The overall agreement between experiment and theory is seen to be very good, but suggestive that the true optical depth in the experiments may be somewhat larger than 6.

VI. SUMMARY

In summary, we have described in detail experiments examining some aspects of coherent wave transport in an ultracold gas of atomic ^{85}Rb. In particular, we have made detailed measurements of the polarization-dependent spatial shape and enhancement factor of the coherent backscattering cone. We have found that for each of the four polarization channels the enhancement factor for the coherent backscattering cones is in good accord with previous work. However, the widths of the cones are significantly different, reflecting the recently predicted sample-size dependence of this quantity [18]. This was made possible by careful measurements of the dimensions of the MOT sample. In addition, we have reported the variation of the relative total intensity of backscattered light as a function of detuning from atomic resonance. The measurements confirm earlier studies which showed that there is a quantum statistical breakdown of reciprocity in light propagating in a near-resonant atomic vapor. In the present work, we also have made detailed measurements of the sample size and shape, and compared the CBS measurements to quantum Monte Carlo simulations of the coherent wave scattering made under nearly identical conditions. The agreement between the results shows that it is possible, by inclusion of up to 20 scattering orders, to accurately model the coherent multiple-scattering wave process.

ACKNOWLEDGMENTS

We acknowledge helpful discussions with Robin Kaiser (INLN, Nice, France). Financial support for this research has been provided by the National Science Foundation (Grant No. NSF-PHY-0099587), by the North Atlantic Treaty Organization (Grant No. PST-CLG-978468), by the Russian Foundation for Basic Research (Grant No. 01-02-17059), and by INTAS (Grant No. INFO 00-479). D.V.K. would like to acknowledge financial support from the Delzell Foundation, Inc.

[1] Ping Sheng, *Introduction to Wave Scattering, Localization, and Mesoscopic Phenomena* (Academic Press, San Diego, 1995).
[2] *Scattering and Localization of Classical waves in Random Media*, edited by P. Sheng (World Scientific, Singapore, 1990).
[3] G. Labeyrie, F. de Tomasi, J.-C. Bernard, C.A. Muller, C. Miniatura, and R. Kaiser, Phys. Rev. Lett. **83**, 5266 (1999).
[4] J. Ishimaru and Y. Kuga, J. Opt. Soc. Am. A **1**, 813 (1984).
[5] P.E. Wolf and G. Maret, Phys. Rev. Lett. **55**, 2696 (1985).
[6] M.P. VanAlbada and A. Lagendijk, Phys. Rev. Lett. **55**, 2692 (1985).
[7] A.A. Golubentsev, Zh. Eksp. Teor. Fiz. **86**, 47 (1984) [Sov. Phys. JETP **59**, 26 (1984)].
[8] Peter Stollmann, *Caught by Disorder: Bound States in Random Media* (Birkhäuser, Boston, 2001).
[9] Ad Lagendijk and B.A. van Tiggelen, Phys. Rep. **270**, 143 (1996).
[10] D.S. Wiersma, P. Bartolini, Ad Lagendijk, and R. Righini, Nature (London) **390**, 671 (1997).
[11] A.A. Chabanov, M. Stoytchev, and A.Z. Genack, Nature (London) **404**, 850 (2000).
[12] H. Cao, J.Y. Xu, D.Z. Zhang, S.H. Chang, T.S. Ho, E.W. Seelig, X. Liu, and R. Cheng, Phys. Rev. Lett. **84**, 5584 (2000); D.S. Wiersma, M.P. van Albada, and Ad Lagendijk, *ibid.* **75**, 1739 (1995).
[13] C. Cohen-Tannoudju and S. Reynaud, Philos. Trans. R. Soc. London, Ser. A **293**, 223 (1979).
[14] B.R. Mollow, Phys. Rev. **178**, 1969 (1969).
[15] G. Labeyrie, C.A. Müller, D.S. Wiersma, Ch. Miniatura, and R. Kaiser, J. Opt. B: Quantum Semiclassical Opt. **2**, 672 (2000).
[16] T. Jonckheere, C.A. Müller, R. Kaiser, Ch. Miniatura, and D. Delande, Phys. Rev. Lett. **85**, 4269 (2000).
[17] C.A. Müller, T. Jonckheere, C. Miniatura, and D. Delande, Phys. Rev. A **64**, 053804 (2001).
[18] D.V. Kupriyanov, I.M. Sokolov, P. Kulatunga, C.I. Sukenik, and M.D. Havey, Phys. Rev. A **67**, 013814 (2003).
[19] M. D. Havey, D. V. Kupriyanov, and I. M. Sokolov (unpublished).
[20] D. Budker, W. Gawlik, D.F. Kimball, S.M. Rochester, V.V. Yashchuk, and A. Weiss, Rev. Mod. Phys. **74**, 1153 (2002).
[21] A. F. Molisch and B. P. Oehry, *Radiation Trapping in Atomic Vapours* (Clarendon Press, Oxford, 1998).

[22] Alan Corney, *Atomic and Laser Spectroscopy* (Clarendon Press, Oxford, 1988); William Happer, Rev. Mod. Phys. **44**, 169 (1972).
[23] A.A. Chabanov and A.Z. Genack, Phys. Rev. Lett. **87**, 153901 (2001).
[24] A.A. Chabanov, M. Stoychev, and A.Z. Genack, Nature (London) **404**, 850 (2002).
[25] Y. Bidel, B. Klappauf, J.C. Bernard, D. Delande, G. Labeyrie, C. Miniatura, D. Wilkowski, and R. Kaiser, Phys. Rev. Lett. **88**, 203902 (2002).